Improvement of plasma position control by decoupling of Fast Plasma Position Control coil control and Poloidal Field coil control on JT-60SA

S. Kojima[1], S. Inoue[1], Y. Miyata[1], H. Urano[1], T. Suzuki[1]

[1] *National Institutes for Quantum Science and Technology, Naka, Japan*

Introduction

Superconducting tokamak mainly controls/will control both plasma current (I_p) and the plasma position and shaping (P&S) by using superconducting poloidal field (SCPF) coils as in EAST [1], KSTAR [2], JT-60SA[3] and ITER[4]. However, SCPF coils are difficult to control the fast plasma motion because they have a slow coil current response due to the large inductance. Thus, the in-vessel coils having a fast coil current response due to the normal conductor are equipped in most of the superconducting tokamaks. Especially, the in-vessel coils are used to suppress the vertical plasma motion, which is caused by high elongation κ.The high elongation contributes to obtaining the high-performance plasma, so the elongation of $\kappa_x \sim 1.9$ is planned in JT-60SA [5]. Two in-vessel coils named fast plasma position control (FPPC) coils will be installed behind the stabilizing plate, as shown in Fig. 1.

In a previous study, we developed the FPPC coil control by applying derivative (D) control of magnetic flux gaps between the last closed flux surface (LCFS) and the control points based on the ISO-FLUX scheme using the magnetohydrodynamic equilibrium control simulator (MECS) code. MECS code is a strong tool to simulate the actual plasma control because it calculates the plasma equilibrium with self-consistent including the limitation of power supply [6] and gives the magnetic flux based on the magnetic surface reconstruction by Cauchy condition surface method [7]. We tried the plasma position via the proportional (P) control of magnetic flux gaps also. In the case of applying the P control, SCPF and FPPC coil controls causes the coupling after starting the control based on ISO-FLUX scheme due to the difference of coil current responses in sharing the controlled objects as Fig. 2. In the case of D control, they do not cause the coupling because the derivative component enhances the high-frequency component of magnetic flux gaps. Thus, the natural decoupling is established in the case of D control. It indicates that the frequency-separation of the controlled object by SCPF and FPPC coil controls is effective. Thus, in this study, we develop the frequency-separation

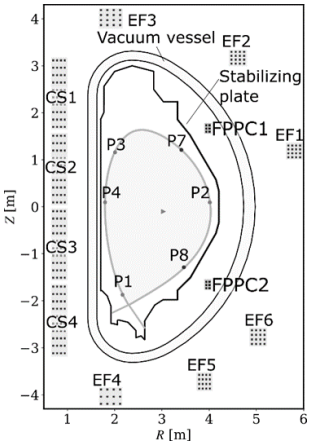

Figure 1: The arrangement of coils and control points in JT-60SA. The superconducting poloidal field, FPPC coils are EF1-6, CS1-4, and FPPC1, 2,respectively.

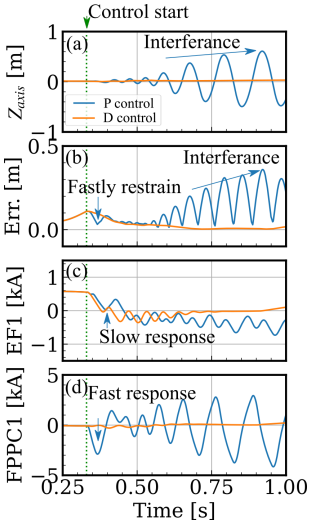

Figure 2: The time evolution of P and D control. The P control shows the interference between SCPF and FPPC coil controls.

between SCPF and FPPC coil controls and evaluate the effectiveness by investigating the frequency transfer function.

Transfer function

In the plasma P&S control based on the ISOFLUX scheme, the deviations of magnetic fluxes between an X point or an attaching point with a limiter ($\psi_{\text{surf.}}$) and the control points ($\boldsymbol{\psi}_{\text{cont.}}(R,Z)$ at P1-4, 7, 8 as shown in Fig. 1) are the controlled objects as $\delta\boldsymbol{\psi}_{\text{s}}(R,Z) = \psi_{\text{surf.}} - \boldsymbol{\psi}_{\text{cont.}}(R,Z)$. In the SCPF coil control, all control points is used. In the FPPC coil control, two control points of P7 and P8 are used for $\delta\boldsymbol{\psi}_{\text{sFP}}$. To evaluate the controllability for vertical direction, we investigated the frequency transfer function by changing the plasma location vertically. Therefore, we changed the reference of all control points like a sine wave $\widetilde{Z_{\text{in}}} = Z_{\text{Amp.}}\sin(2\pi ft)$ with the frequency of $f = 1, 2, 3, 5, 10, 20, 30, 50, 100, 200$ Hz with an amplitude of $Z_{\text{Amp.}} = 1$ cm as shown in Fig.3 (a). The magnetic axis can be regarded as the output of the fluctuation of all control points, as shown in Fig.3 (b). Thus, we can obtain the transfer function as $G_{\text{cont.z}} = \frac{Z_{\text{axis}}}{Z_{\text{fluc.}}}$ and the frequency transfer function as

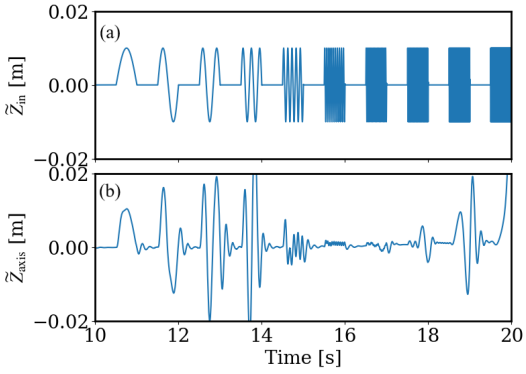

Figure 3: The fluctuation part of (a) the control points Z_{in} and (b) the magnetic axis Z_{axis} in the SCPF coil control.

$$G_{\text{cont.z}}(f) = |G_{\text{cont.z}}(f)|e^{i\angle G_{\text{cont.z}}(f)}. \tag{1}$$

The plasma conditions were fixed at $I_{\text{p}} = 2.5$ MA, the poloidal beta $\beta_{\text{p}} = 0.5$, and the internal inductance $l_{\text{i}} = 0.85$ as the plasma ramp-up. The SCPF coil control uses the proportional integral derivative (PID) control of the magnetic flux gaps. The control gains are gave $G_{\text{SP}} = 0.002$, $G_{\text{SI}} = 0.0016$, $G_{\text{SD}} = 0.001$.

The frequency transfer function's magnitude is defined as $G_g(f) = 20\log_{10}|G_{\text{cont.z}}(f)|$ (Fig.4 (a)). Its phase is defined as $G_{\text{p}}(f) = \angle G_{\text{cont.z}}(f)$ (Fig.4 (b)). The ideal frequency transfer function's magnitude is 0 dB, and its phase is 0 degrees in any frequency. In the case of the SCPF coil control, the frequency transfer function's magnitude is maintained until $\sim$ 7 Hz. The phase delay is started from $\sim$ 5 Hz. The phase delay during the magnitude being constant shows the dead time element of the SCPF coil control. However, the dead time element is not caused by the delay of the command for the power supply because it is relatively short of only 2.25 ms ($\sim$ 440 Hz).

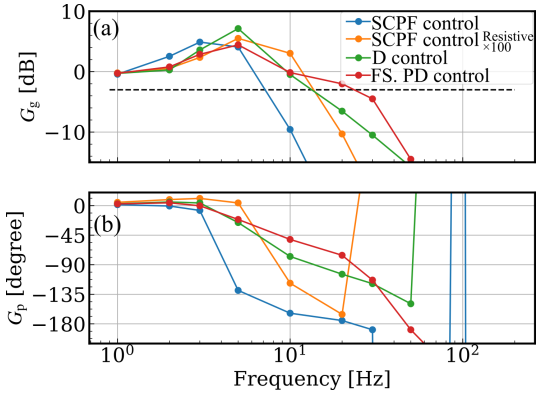

Figure 4: The bode line figure of the transfer function on the frequency axis.

We investigated the lowest effective frequency of the stabilizing plate for plasma by changing the stabilizing plate's resistivity. Larger resistance of the stabilizing plate, the lowest effective frequency is higher. If the frequency range affected by the stabilizing plate is overwrapping with the frequency range covered by the coil control, the lowest frequency affected by the stabilizing plate is clear by increasing the resistivity of the stabilizing plate. In the SCPF coil control with the stabilizing plate with 100 times larger resistance, the controllable frequency is expanded until $\sim$ 12 Hz. The phase delay does not occur until 5 Hz. It indicates that the dead time element of SCPF coil control is caused by the stabilizing plate. The stabilizing plate affects until the frequency range, which is controlled by the SCPF coil control. The covering to low frequency by the stabilizing plate is a good advantage for stabilizing plasma, whereas it had a bad influence on plasma control by coils.

In the FPPC coil control, we extracted the high-frequency part of $\delta\boldsymbol{\psi}$ for the control object $\delta\boldsymbol{\psi}_{\mathrm{fast}}$ by the high-pass filter to establish the frequency-separation. The high-pass filter is designed by subtracting the numerical low-pass filtered $\delta\boldsymbol{\psi}$ from the original $\delta\boldsymbol{\psi}$. We applied the numerical low-pass filter using the convolution integration of the inversed FFT function because the low-pass filter is reliable for the low sampling discrete signal. The derivative component of magnetic flux gap was also added in the control. We named it the frequency-separated PD control as

$$\delta\boldsymbol{\psi}_{\mathrm{FP}} = G_{\mathrm{P_{FP}}}(\delta\boldsymbol{\psi}_{\mathrm{fast}} + T_{\mathrm{D}}\frac{\mathrm{d}\delta\boldsymbol{\psi}_{\mathrm{sFP}}}{\mathrm{d}t}). \tag{2}$$

The control gains for the frequency-separated PD control were fixed at $G_{\mathrm{P_{FP}}} = 1/64$, $T_{\mathrm{D}} = 0.00025$. The cut-off frequency of the low-pass filter was set at $\sim$ 50 Hz to avoid the coupling with the SCPF coil control. In the case of the D control as $\delta\boldsymbol{\psi}_{\mathrm{FP}} = G_{\mathrm{P_{FP}}}T_{\mathrm{D}}\frac{\mathrm{d}\delta\boldsymbol{\psi}_{\mathrm{sFP}}}{\mathrm{d}t}$, the fluctuation until $\sim$12 Hz could be sustained (Fig.4 (a)); however, in the case of the frequency-separated PD control, the control improved to keep the fluctuation until $\sim$ 22 Hz. By applying the frequency-separated PD control, the controllabilitiy for the high-frequency plasma fluctuation expands than the D control. The phase delay is also restrained by applying the frequency-separated PD control (Fig.4 (b)). The effectiveness of the frequency-separated PD control in less effect of the stabilizing plate was also investigated because the frequency range covered by the stabilizing plate is around a few Hz. In that case, the plasma position control followed until $\sim$ 50 Hz. We can see that the stabilizing plate plays as the filter for the plasma control by coils.

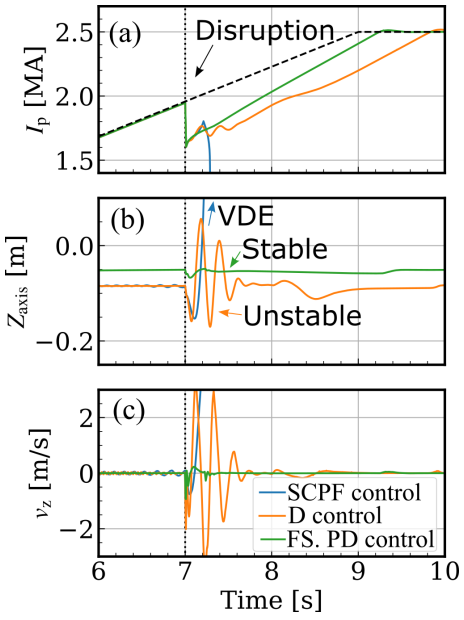

Figure 5: The time evolutions of (a) I_{p}, (b)Z_{axis}, (c) vertical velocity v_{z} in I_{p} disruption.

Plasma operation region in plasma ramp-up

We can expect the stable control by applying the frequency-separated PD control. Thus, the controllability for the elongation and the I_p disruption intensity was investigated. The I_p disruption enhances the vertical instability by reducing the stabilizing effect of the stabilizing plate due to departing from the stabilizing plate. We causes I_p disruption during the plasma ramp-up phase at $I_p \sim 2$ MA with $\beta_p = 0.5$ and $l_i = 0.85$. An example of the plasma controls during I_p disruption is shown in Fig. 5. In the case of the SCPF coil control, the vertical displacement event occurs. The FPPC coil control is required to sustain the plasma. In the case of the D control, the stabilization takes to time more than applying the frequency-separated PD control. In the frequency-separated PD control, the plasma location change is restrained without the coupling the SCPF coil control. The controllability for the elongation plasma in various I_p disruption intensities is shown in Fig. 6. In the SCPF coil control, the highest elongation was $\kappa \sim 1.65$ without the I_p disruption. In the D control, the highest elongation was $\kappa_x \sim 1.77$ without the I_p disruption. The frequency-separated PD control achieved the highest elongation $\kappa_x \sim 1.9$ without the I_p disruption, which is limited by the limiter structure. In addition, the I_p disruption of 10 % can be sustained. In the elongation of $\kappa_x \sim 1.6$, the I_p disruption of ~ 32 % (~ 600 kA drop) is acceptable. The frequency-separation between the SCPF and FPPC coil controls can expand the stable plasma operation region.

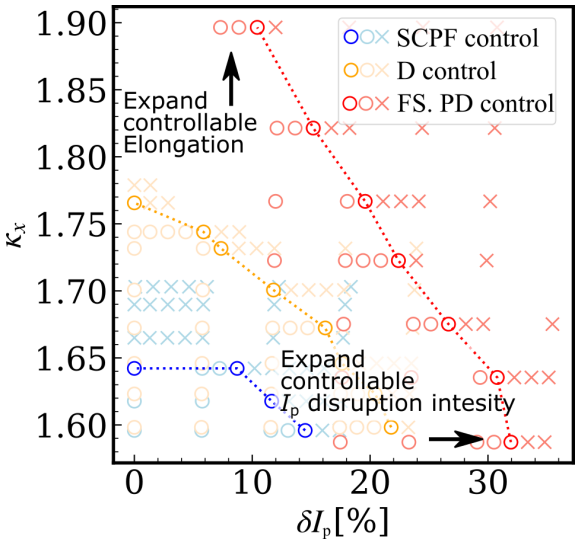

Figure 6: The map of the controllable elongation and I_p disruption. The succussed and failed operations are marked by cycle and cross.

Summary

The coil current responses are different in SCPF coils and FPPC coils. It causes the coupling between SCPF and FPPC coil control. Thus, the frequency-separation between those controls is applied by adding the high-pass filter for the controlled object by the FPPC coil control. The frequency-separation between SCPF and FPPC coil controls establishes the decoupling between SCPF and the FPPC coil controls. It expands the frequency range controlled by coils. In the case of the frequency-separated PD control, the stabilization of plasma caused by I_p disruption has a better performance than applying the D control. Consequently, the FPPC coil control with the frequency-separated PD control can achieve higher elongation $\kappa_x \sim 1.9$ with extra margin for I_p disruption. The improved FPPC coil control will safely operate the plasma according to the scenarios in JT-60SA.

References

[1] Y. Guo et al., Nucl. Fusion **60** 076002 (2020)
[2] D. Muller et al., Fusion Eng. and Des. **141** 9 (2019)
[3] S. Inoue et al., Nucl. Fusion **61** 096009 (2021)
[4] Y. Gribov et al., Nucl. Fusion **50** 073021 (2015)
[5] JT-60SA Research Plan - Version 4.0, Sept. (2018)
[6] Y. Miyata et al. , Plasma and Fusion Research **9** 3403045 (2014)
[7] Y. Miyata et al. Rev. Sci. Instrum. **86** 073511 (2015)